Journal Pre-proof

Thermodynamic modeling of the U_3O_{8-x} solid solution

Stephen A. Utlak, Jacob W. McMurray

PII: S0022-3115(19)30996-1

DOI: https://doi.org/10.1016/j.jnucmat.2019.151844

Reference: NUMA 151844

To appear in: *Journal of Nuclear Materials*

Received Date: 29 July 2019

Revised Date: 9 October 2019

Accepted Date: 10 October 2019

Please cite this article as: S.A. Utlak, J.W. McMurray, Thermodynamic modeling of the U_3O_{8-x} solid solution, *Journal of Nuclear Materials* (2019), doi: https://doi.org/10.1016/j.jnucmat.2019.151844.

Title: Thermodynamic modeling of the U_3O_{8-x} solid solution

Authors: Stephen A. Utlak[ab] and Jacob W. McMurray[c]

[a] Materials Science and Technology Division, Oak Ridge National Laboratory, 1 Bethel Valley Rd, Oak Ridge, TN 37830 (email: utlaksa@ornl.gov)

[b] Corresponding author

[c] Materials Science and Technology Division, Oak Ridge National Laboratory, 1 Bethel Valley Rd, Oak Ridge, TN 37830 (email: mcmurrayjw1@ornl.gov)

Abstract

It is important to accurately characterize the equilibrium behavior of U_3O_8 as the determination of the oxygen to uranium ratio in UO_2 powders and pellets is dependent on U_3O_8 stoichiometry. Prior thermodynamic modeling efforts have treated U_3O_8 as stoichiometric, however it is experimentally known that the phase exhibits hypostoichiometric solubility behavior at temperatures > 850 K. Thus, the goal of this work was to model U_3O_8 as a solid solution using the compound energy formalism and optimize the model to experimental data according to the CALPHAD methodology. Results of the U_3O_{8-x} model assessment were visualized by recalculating the previously assessed U-O binary system phase diagram replacing stoichiometric U_3O_8 with a U_3O_{8-x} solid solution model, and a recommendation is made to revise the U_3O_8 to uranium conversion factor used in the ASTM C 1453 standard based on the literature and updated thermodynamic representation for U_3O_{8-x} presented in this work.

Keywords

Nuclear fuel, UO_2, U_3O_8, thermodynamics, CALPHAD, modeling

1. Introduction

U_3O_8 is an important phase used in the production of urania (UO_2) nuclear fuel pellets as a majority of yellowcake consists of U_3O_8[1, 2] and U_3O_8 can be used to verify the oxygen composition UO_2. As is well understood, UO_2 exhibits oxygen homogeneity and is more correctly represented by the formula $UO_{2\pm x}$.[3, 4] The ASTM C 1453 standard (C1453)[5] for determining x, or the oxygen to uranium ratio (O/U) in nuclear grade $UO_{2\pm x,}$ calls for the material to be calcined in air in order to use U_3O_8 as a reference. The O/U is then calculated from the weight gain.[5] However, U_3O_8 has been shown to exhibit hypostoichiometry[6, 7 8-14] and should be expressed as U_3O_{8-x}. Like $UO_{2\pm x}$, it also has a complex relationship with the oxygen potential of the atmosphere. Hence, having an accurate understanding of U_3O_{8-x} phase behavior at equilibrium is necessary to ensure that conversion factors using U_3O_{8-x} are correct.

As noted, experimental studies[6, 7 8-14] have indicated that U_3O_{8-x} has a range of hypostoichiometric solubility at > 850 K, however previous modeling efforts have treated the phase stoichiometrically.[3, 4] Similarly, C1453[5] established the test method to determine the uranium content in nuclear grade UO_2 power and pellets assumes stoichiometric U_3O_{8-x} at 1173 K for the U_3O_8 to uranium conversion factor. Accounting for the nonstoichiometry of U_3O_{8-x} will improve the characterization of the equilibrium behavior of U_3O_8 in the U-O system and provide a conversion factor for more accurate O/U determinations for $UO_{2\pm x}$.

Accordingly, this work reports on modeling the U_3O_{8-x} phase as a solid solution using the compound energy formalism[15-20] (CEF), which is optimized to experimental data according to the calculation of phase diagrams (CALPHAD) methodology[21] using the FactSage software.[22] Calculations with the U_3O_{8-x} model are performed and compared to experimental data to verify accuracy, and the U-O phase diagram was recalculated with the U_3O_{8-x} solid solution phase. The updated model allows for determining x in the U_3O_{8-x} reference phase as a function of temperature and oxygen partial pressure in order to more correctly calculate the O/U in $UO_{2\pm x}$ nuclear grade fuel powder and pellets.

2. Literature review

2.1. U_3O_8 crystalline structure

Four U_3O_8 polymorphs were experimentally identified by Naito et al.[23, 24] Studies[25-28] have established that the highest temperature polymorph, which will be modeled in this work, has a hexagonal crystalline structure.

Loopstra[29] employed neutron diffraction to resolve discrepancies between experimental U_3O_8 crystalline structure results reported by Zachariasen,[30] Chodura & Maly,[31] and Andresen,[32] in which it was determined that at room temperature two uranium atoms labeled as U(1) and U(2) are each surrounded by six oxygen atoms at distances between 2.07 to 2.23 Å with seventh oxygen atoms bonded to U(1) and U(2) at distances of 2.44 and 2.71 Å, respectively. Later, Loopstra[26] established that the room temperature orthorhombic and high temperature hexagonal structures are very similar with the main difference as observed by Ball & Dickens[33] being that the hexagonal form has one uranium site whereas the orthorhombic structure has two. However, the surrounding oxygens are approximately equivalent for both lattice types.[26, 33]

It was also postulated by Loopstra[29] that U(1) and U(2) could be identified as the U^{+6} and U^{+5} cations, respectively. As summarized by Brincat et al,[34] while some early experimental investigations contradicted this assumption by indicating U(1) and U(2) valence states of +6 and +4, more recent experimental studies conducted by Kvashnina et al[35] and Teterin & Teterin[36] clarified that +6 and +5 were the most stable arrangement. Additionally, ab initio DFT + U computations[33] determined that U_3O_8 with U^{+5}/U^{+6} yielded the most stable crystalline structure.

2.2. U_3O_{8-x} solubility

The solubility range of U_3O_{8-x} has been experimentally established as approximately $2.60 < O/U < 2.67$.[6-8, 11, 37] Studies have postulated that the nonstoichiometry mechanism of U_3O_{8-x} consists of only oxygen vacancies[30, 38] or vacancies and interstitials.[39, 40] Ackerman & Chang[7] noted that vacancy formation may drive nonstoichiometry at lower temperatures but that a more complex mechanism may occur at higher temperatures although this mechanism was not hypothesized. Ball & Dickens[33] used atomistic simulation

techniques to analyze defect energetics to conclude that uranium interstitial ions are unstable with respect to their movement onto normal lattice sites and the resulting formation of oxygen vacancies, and consequently concluded that the most favorable defect mechanism is oxygen vacancy formation.

2.3. U_3O_{8-x} experimental data

Many experimental studies[6, 7 8-14] have conducted measurements to determine the hypostoichiometric solubility of U_3O_{8-x}. Of these, Caneiro & Abriata[41] reported the existence of a U_8O_{21+x} phase that formed a two phase region with U_3O_{8-x} in the range of $2.655 < O/U < 2.67$. Labroche et al,[42] however, rejected the observation that the U_8O_{21+x} phase is stable at equilibrium citing kinetic limitations in the Caneiro & Abriata[41] study. For this work, the conclusion of Labroche et al[42] that U_8O_{21+x} is metastable is assumed. Therefore, the results of Caneiro & Abriata[41] as well as Dharwadkar et al[12] that also reported observation of the U_8O_{21+x} phase was neglected. Similarly, the thermobalance measurements of Fujino et al[10] exhibited the same non-reversible hysteresis as Caneiro & Abriata[41] and Dharwadkar et al,[12] hence these measurements were also disregarded. All other experimental solubility data were consistent except for measurements of by Gronvold,[9] which had too high uncertainty for use in optimizing the adjustable model parameters.

Ackerman & Chang[7] determined solubility limits of U_3O_{8-x} by measuring partial pressures of O_2 at different isotherms of U_3O_{8-x}, hence this partial pressure data was also considered when developing the U_3O_{8-x} model. An earlier study conducted by Kotlar et al[13] similarly measured O_2 partial pressure, however their results significantly differed from Ackerman & Chang[7] at comparable temperatures. As the data of Ackerman & Change[7] are consistent with other studies,[6, 8, 11, 37] the Kotlar et al[13] measurements have been neglected.

Inaba et al[37] measured the heat capacity of $UO_{2.667}$ up to 970 K and reported a second order phase transition at 850 K. This phase transition temperature as well as the measured heat capacity data were both incorporated into the U_3O_{8-x} model assessment.

3. Thermodynamic modeling and optimization

3.1. U-O system

Guéneau et al[3, 4] previously assessed the U-O system while treating U_3O_8 as four stoichiometric compounds, hence all compounds, gas species, and the liquid were adopted from those assessments except for the highest temperature polymorph of U_3O_8, which was replaced with the U_3O_{8-x} CEF model developed in this work.

3.2. CEF model

The U_3O_{8-x} solid solution was modeled using the CEF with the three sublattice structure:

$$(U^{+5}, U^{+6})^{\alpha}_{15}[O^{-2}]_{39}\{O^{-2}, Va\}^{\beta}_{1}$$

The first and second sublattices represent the uranium and oxygen lattice sites in the U_3O_8 crystalline structure as described in Section 2.1 whereas the third accounts for the mechanism of U_3O_{8-x} nonstoichiometry in which a vacancy substitutes for an O^{-2} species. As discussed in Section 2.1., U^{+5} and U^{+6} result in the most stable U_3O_{8-x} crystalline arrangement, thus these are the cations selected to occupy the first sublattice.

The sublattice stoichiometric coefficients account for the complete U_3O_{8-x} solubility range of $2.60 < O/U < 2.67$.

3.2.1. Optimization

To limit a degree of freedom during the optimization procedure of the U_3O_{8-x} model, the Gibbs energies of the two valence states of the $U_{15}O_{39}$ and $U_{15}O_{40}$ endmembers were set as equivalent (Table 1).

The U_3O_{8-x} CEF model was initially optimized to the heat capacity data of Inaba et al[37] through adjustment of the 'b' term of the heat capacity polynomial of the two $U_{15}O_{39}$ endmembers (Table 2). Redlich-Kister interaction parameters as well as the standard enthalpy and entropy of all U_3O_{8-x} endmembers were then optimized to the O_2 partial pressure data reported by Ackerman & Chang[7] and U_3O_{8-x} solubility data measured by multiple studies.[6-8, 11, 37]

The resulting CEF Gibbs energy function is shown in eq. (1) with parameter values listed in Table 1.

$$G_{\mathrm{m}}^{\mathrm{U_3O_{8-x}}} = y_{\mathrm{U^{+5}}}^{\alpha} y_{\mathrm{O^{-2}}}^{\beta}\,{}^{\mathrm{o}}G_{\mathrm{U_{15}O_{40}^{-5}}} + y_{\mathrm{U^{+6}}}^{\alpha} y_{\mathrm{O^{-2}}}^{\beta}\,{}^{\mathrm{o}}G_{\mathrm{U_{15}O_{40}^{+10}}} + y_{\mathrm{U^{+5}}}^{\alpha} y_{\mathrm{Va}}^{\beta}\,{}^{\mathrm{o}}G_{\mathrm{U_{15}O_{39}^{-3}}} + y_{\mathrm{U^{+6}}}^{\alpha} y_{\mathrm{Va}}^{\beta}\,{}^{\mathrm{o}}G_{\mathrm{U_{15}O_{39}^{+12}}} \quad \text{Eq. (1)}$$
$$+ RT\left[15\left(y_{\mathrm{U^{+5}}}^{\alpha}\ln y_{\mathrm{U^{+5}}}^{\alpha} + y_{\mathrm{U^{+6}}}^{\alpha}\ln y_{\mathrm{U^{+6}}}^{\alpha}\right) + y_{\mathrm{O^{-2}}}^{\beta}\ln y_{\mathrm{O^{-2}}}^{\beta} + y_{\mathrm{Va}}^{\beta}\ln y_{\mathrm{Va}}^{\beta}\right]$$
$$+ y_{\mathrm{U^{+5}}}^{\alpha} y_{\mathrm{U^{+6}}}^{\alpha} y_{\mathrm{O^{-2}}}^{\beta}\left({}^{0}L_{\mathrm{U^{+5},U^{+6}:O^{-2}:O^{-2}}} + {}^{1}L_{\mathrm{U^{+5},U^{+6}:O^{-2}:O^{-2}}} + {}^{2}L_{\mathrm{U^{+5},U^{+6}:O^{-2}:O^{-2}}}\right)$$
$$+ y_{\mathrm{U^{+5}}}^{\alpha} y_{\mathrm{U^{+6}}}^{\alpha} y_{\mathrm{Va}}^{\beta}\left({}^{0}L_{\mathrm{U^{+5},U^{+6}:O^{-2}:Va}} + {}^{1}L_{\mathrm{U^{+5},U^{+6}:O^{-2}:Va}} + {}^{2}L_{\mathrm{U^{+5},U^{+6}:O^{-2}:Va}}\right)$$

4. Results and discussion

4.1. U_3O_{8-x} heat capacity

Heat capacity measurements were conducted by Inaba et al[37] for $UO_{2.667}$. It was necessary, however, to calculate the corresponding heat capacity curve shown in Fig. 1 at $UO_{2.6638}$ as the computed upper U_3O_{8-x} solubility limit at the maximum temperature considered by Inaba et al[37] of 970 K lies at an O/U of 2.6638 (Fig. 2). The difference in stoichiometries is minimal, thus experimental data and model calculations could be compared for validation of model optimization accuracy.

Inaba et al[37] observed $UO_{2.667}$ heat capacity λ-type phase transitions at temperatures of 483, 568 and 850 K. As the lower temperature U_3O_8 polymorphs are treated as stoichiometric compounds, the computed $UO_{2.6638}$ heat capacity behavior at < 760 K in Fig. 1 is governed by the U_3O_8 compound heat capacity polynomials derived by Guéneau et al[3, 4] These polynomials have been developed to represent a smooth curve, hence no λ transitions are calculated at < 760 K. The small increase in $UO_{2.6638}$ heat capacity and entropy at 654 K is a result of initial U_3O_{8-x} phase formation (Fig. 2), however as this is a two-phase region, phase transformation heat capacity behavior is appropriately absent from Fig. 1 at 654 K. At approximately 760 K, model calculations in Fig. 1 indicate the start of a peak formation representing the initiation of the phase transition from $U_3O_8(\gamma)$ to the high-temperature U_3O_{8-x} solid solution. Behavior of this peak is characteristic of a λ transition[43] agreeing with the observation of Inaba et al[37] As noted by Dorogokupets,[43] λ transitions can be approximated as first-order transitions, which aligns with the $UO_{2.6638}$ entropic behavior at ~ 850 K that approximates a jump discontinuity associated with the phase transition latent heat (Fig. 3).[44] This entropic jump discontinuity results in a singularity of the derivative heat capacity at 850 K (Fig. 1) in accordance with the theory of first-order phase

transitions.[44] Thus, while Inaba et al[37] did not conclude the nature of the 850 K phase transition, the calculated $UO_{2.6638}$ heat capacity indicates that the $U_3O_8(\gamma)$ to U_3O_{8-x} phase transition is first-order.

The $UO_{2.667}$ heat capacity predicted by Guéneau et al[3, 4] from four stoichiometric U_3O_8 polymorphs is superimposed in Fig. 1 for comparison with the heat capacity calculated using the U_3O_{8-x} model. Both calculated heat capacities are less than the Inaba et al[37] measurements at > 850 K (Fig .1). The experimental data is elevated likely due to the presence of gaseous species in addition to U_3O_{8-x} in the Inaba et al[37] measurements as U_3O_{8-x} is hypostoichiometric at an O/U of 2.667 and temperatures > 850 K (Fig. 2). Hence, as the computed heat capacities agree well (Fig. 1), it can be concluded that the U_3O_{8-x} C_p has been successfully optimized.

4.2. U_3O_{8-x} solubility

Fig. 2 shows the calculated solubility range of the U_3O_{8-x} model with experimental phase data superimposed for comparison. The computed 850 K formation temperature of the U_3O_{8-x} phase at the O/U of 2.667 agrees well with the experimentally measured temperatures of 843 K and 850 K reported by Ackerman & Chang[7] and Inaba et al,[37] respectively. A similar good agreement was obtained between the calculated and experimentally measured U_3O_{8-x} lower solubility limit of approximately 2.605 O/U at 1325 K. The calculated U_3O_{8-x} upper solubility limit shows some discrepancy with solubility measurements from 1160 to 1445 K, which was the best obtained agreement when optimizing the U_3O_{8-x} model to both solubility data as well as the partial pressure of O_2 measurements reported by Ackerman & Chang.[7]

A U_3O_{8-x} peritectoid point was computed to form at 2.628 O/U and 2236 K, which was an increase in temperature from the stoichiometric U_3O_8 to UO_{2+x} + gas invariant transition temperature of approximately 2004 K calculated by Guéneau et al.[4] No experimental data has been reported for this invariant point, hence the increase is acceptable and may be an improved prediction as the model is based on more physics compared to a purely stoichiometric high temperature U_3O_8.

The calculated U_3O_{8-x} eutectoid point at 2.623 O/U and 656 K also required estimation due to lack of experimental data. It is likely that the U_3O_{8-x} lower solubility boundary would continue at < 656 K and extend to the lower temperature U_3O_8 polymorphs, hence it may be of interest for a future work to

develop solid solution models for these polymorphs. This effort would likely first require additional experimental measurements similar to those conducted by Ackerman & Chang[7] for use in assessing the U_3O_{8-x} lower temperature solubility behavior.

4.3. Partial pressure of O_2 for isotherms of U_3O_{8-x}

In addition to solubility experimental data, the partial pressure of O_2 for different isotherms of U_3O_{8-x} measured by Ackerman & Chang[7] was also included in the U_3O_{8-x} model optimization. Comparison of the model calculations and corresponding experimental data shown in Fig. 4 indicates overall good agreement. Certain computed curves such as at 1319 K showed a minor increase in discrepancy with data in comparison to the curve at 965 K, however all experimental data is sufficiently predicted by the U_3O_{8-x} CEF model.

4.4. Recalculation of U-O phase diagram

Fig. 5 shows a recalculation of the U-O phase diagram with the U_3O_{8-x} solid solution phase assessed in this work; all other compounds, gas species, and the liquid phase were adopted from Guéneau et al.[3, 4] Visualizing the U_3O_{8-x} phase within the U-O system provides perspective on the relatively narrow phase solubility region. Fig. 2 indicates, however, that despite this small solubility range, the U_3O_{8-x} model well predicts experimental upper and lower solubility limits while maintaining consistency with the phase equilibria presented by Gueneau et al[3, 4] and the experimental work on which it is based.

4.5. Revision of ASTM C 1453 standard

C1453[5] establishes a calculation procedure to determine the uranium content in nuclear grade UO_2 powder and pellets, which involves the use of a U_3O_8 to uranium conversion factor for natural uranium defined by eq. 2:

$$\text{Conversion Factor} = \frac{3A}{3A + 8O} \qquad \text{Eq. (2)}$$

where A and O are the atomic weights of uranium and oxygen, respectively. The value of 8 in the denominator is based on stoichiometric U_3O_8, however, as indicated by Figs. 2 & 5, U_3O_{8-x} is

hypostoichiometric at 1173 K. According to C1453,[5] the process of converting UO_2 to U_3O_8 occurs by ignition at 1173 ± 25 K in air.

This reaction can be written as:

$X \cdot UO_2(s) + 0.21 \cdot O_2(g) \rightarrow Y \cdot U_3O_{8-x}(s) + Z \cdot O_2(g)$

where X, Y, and Z are the molar amounts of reactant and products, respectively. The moles of the O_2 reactant is equivalent to 0.21 as ignition of UO_2 occurs in air.[5] Other elemental gaseous species in air[45] were neglected as these are not likely to react with UO_2.[46-48]

C1453[5] recommends transferring 2 to 12 grams of UO_2 powder or pellets to a platinum crucible, which convert to $7.407 \cdot 10^3$ and 0.044 mol UO_2, respectively, and are the values of X in the above reaction. Hence, the reactant amounts including 0.21 mol $O_2(g)$ equate to O mole fractions of 0.983 and 0.92, respectively, which lie in the region of U_3O_{8-x} + Gas in Fig. 5. Consequently, the molar amount of U_3O_{8-x} yielded from the reaction will be given by the upper U_3O_{8-x} phase boundary (Figs. 2 & 5).

As the standard[5] indicates an ignition temperature uncertainty range of ± 25 K, Table 3 shows results of calculated O stoichiometry for the $U3O_{8-x}$ phase at temperatures of 1148, 1173, and 1198 K. Averaging the computed O stoichiometries at the three ignition temperatures provides a reasonable estimation of the U_3O_{8-x} hypostoichiometry and is equivalent to 7.9469. As a result of this revision, if it is assumed that the uranium isotopic abundance does not deviate from natural uranium, the C1453[5] U_3O_8 uranium conversion factor should be revised from 0.8480 to 0.8489.

5. Conclusion

A thermodynamic model of the U_3O_{8-x} solid solution phase has been developed using the CEF and optimized in accordance with the CALPHAD methodology to experimental measurements of U_3O_{8-x} heat capacity and phase solubility as well as the partial pressure of O_2 in the U-O system. Calculations with the assessed model agreed well with experimental data, and the U-O phase diagram was recalculated with the U_3O_{8-x} solid solution phase. While the high temperature U_3O_{8-x} polymorph has now been modeled as a solid solution, future work should focus on investigating determining if the lower temperature U_3O_8 polymorphs exist as solid solutions requiring experimental measurements.

Based on the experimental studies reviewed in this work as well as the development of a physics-based U_3O_{8-x} thermodynamic model that agrees well with those data, it is recommended that C1453[5] be revised to account for the hypostoichiometric solubility of U_3O_{8-x}. While the current conversion factor for O/U in C1453[5] uses a value of 0.8480 based on stoichiometric U_3O_8., it is recommended that, assuming the uranium isotopic abundance does not deviate from natural uranium, the value be revised to 0.8489 to account for the oxygen hypostoichiometry of U_3O_{8-x} at 1173 K.

Acknowledgements

The authors wish to acknowledge the technical insight of Dr. Stephen Raiman and Dr. Ying Yang at ORNL.

Funding: This paper was supported by the Advanced Fuels Campaign of the Nuclear Technology Research and Development program in the Office of Nuclear Energy, US Department of Energy.

6. Figures & captions

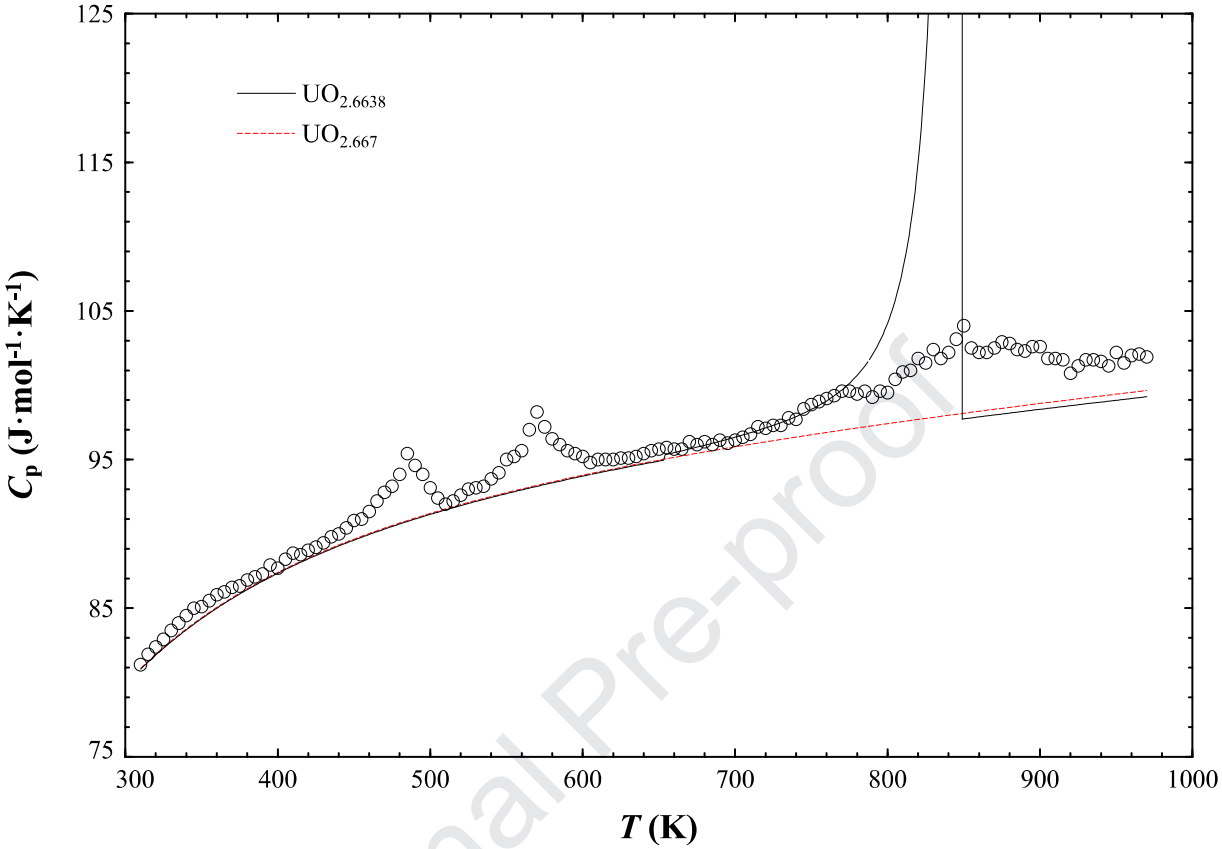

Fig. 1. Heat capacities of $UO_{2.6638}$ and $UO_{2.667}$ computed with inclusion of, respectively, the U_3O_{8-x} model and four U_3O_8 stoichiometric polymorphs derived by Guenuea et al.[3, 4] Experimental $UO_{2.667}$ heat capacity data shown as points was obtained from Inaba et al.[37]

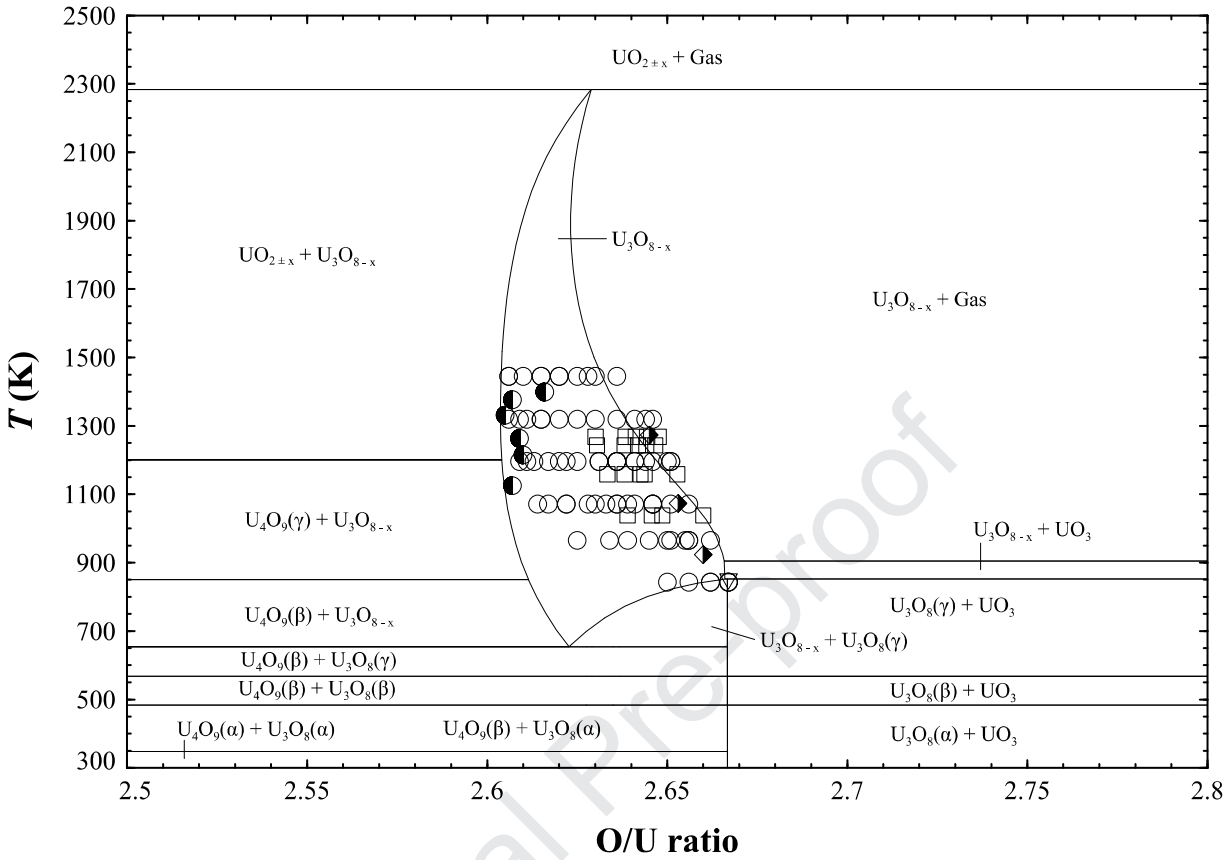

Fig. 2. Computed U_3O_{8-x} solubility region within U-O system with experimental measurements shown as points. Data: ○[7] □[6] ▽[37] ◐[8] ◆[11]

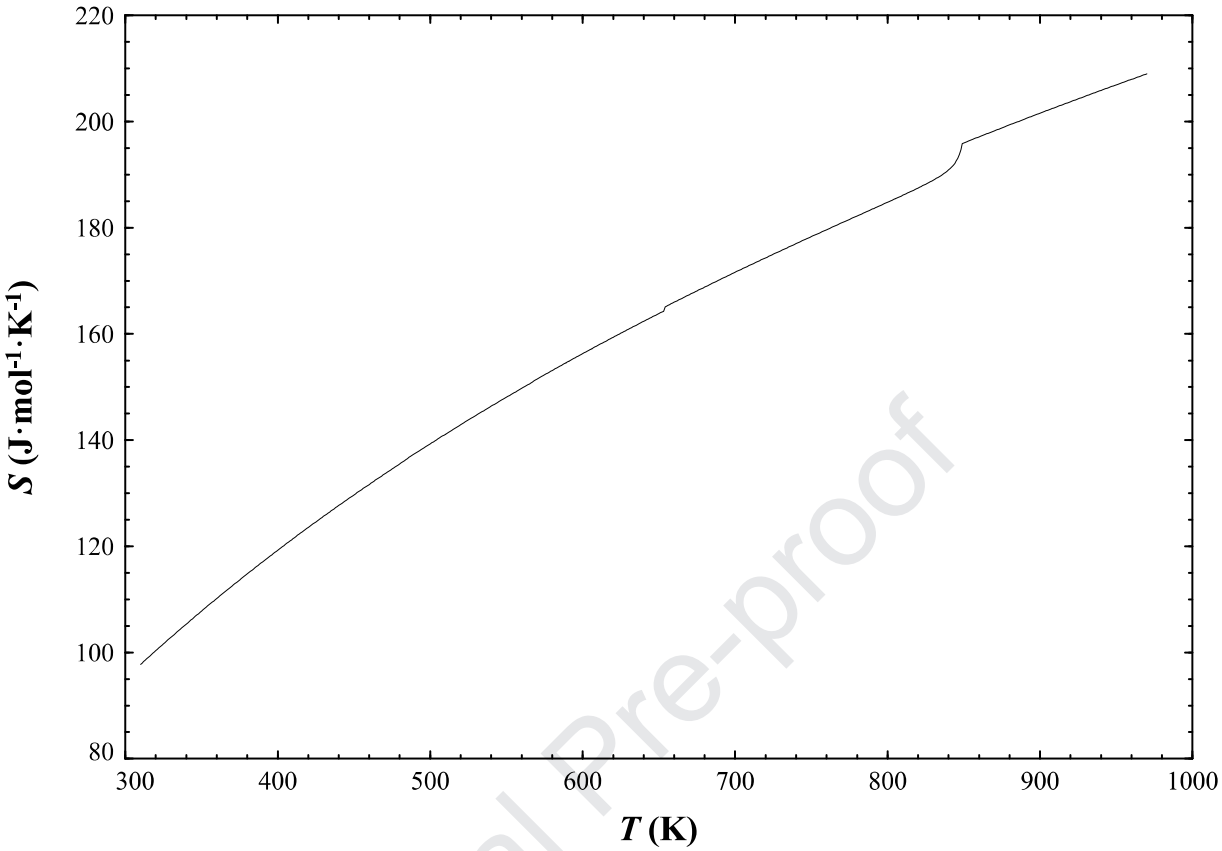

Fig. 3. Computed entropy of $UO_{2.6638}$.

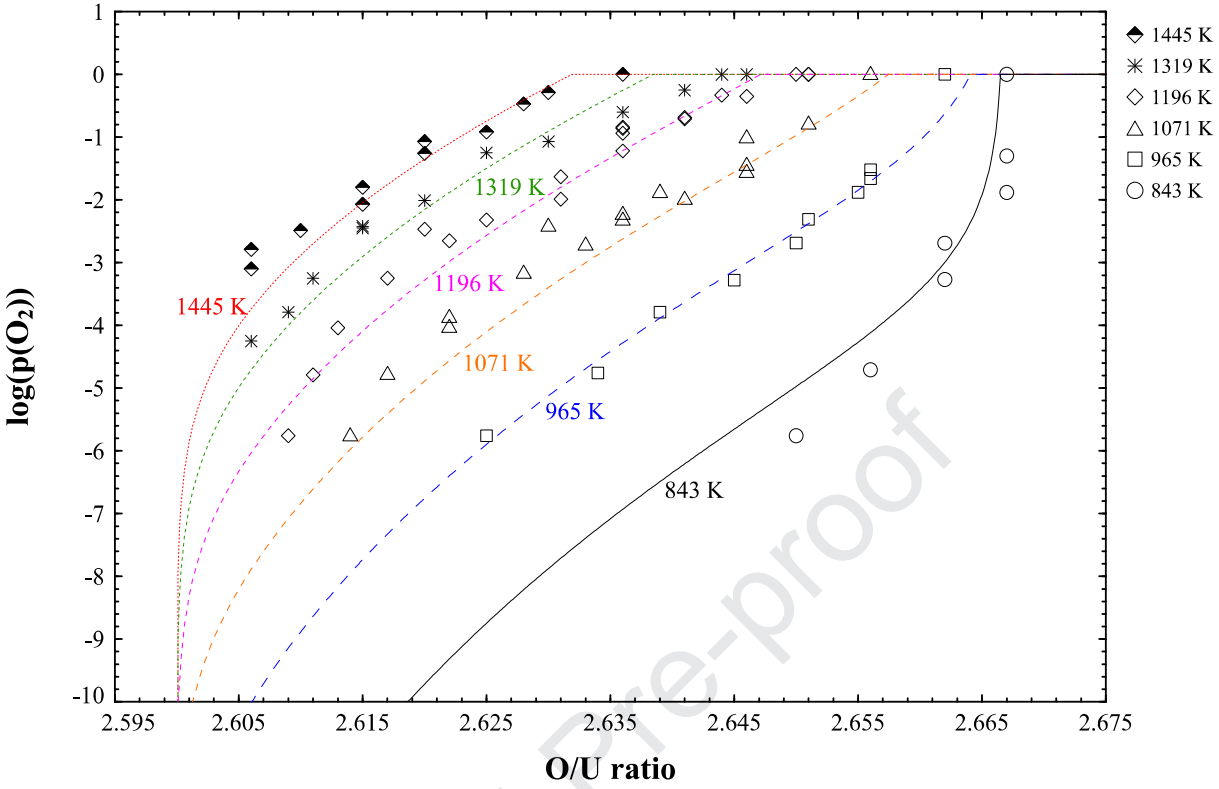

Fig. 4. Computed partial pressures of O_2 for isotherms of U_3O_{8-x} with experimental measurements of Ackerman & Chang[7] shown as points.

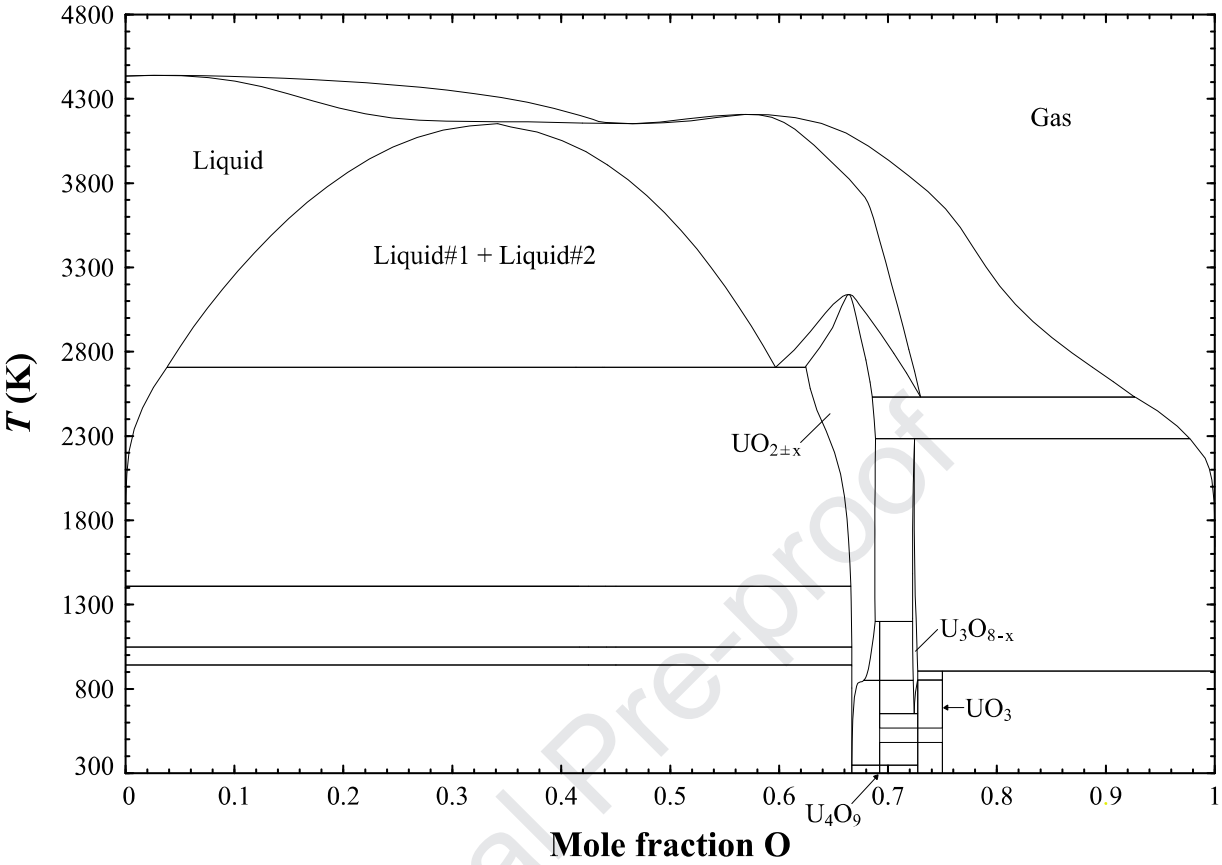

Fig. 5. Recalculated U-O binary system phase diagram from Gueneau et al[3, 4] with inclusion of the U_3O_{8-x} phase assessed in this work.

7. Tables

Table 1. Model parameters for U_3O_{8-x} solid solution (all ^oG and L parameter units are J/mol)[a]

U_3O_{8-x} $(U^{+5},U^{+6})_{15}[O^{-2}]_{39}\{O^{-2},Va\}_1$
${}^oG_{U_{15}O_{40}^{-5}} = {}^oG_{U_{15}O_{40}^{+10}} = 5{}^oG_{U_3O_8(s)} + 7719 + 18T$
${}^oG_{U_{15}O_{39}^{-3}} = {}^oG_{U_{15}O_{39}^{+12}} = 5{}^oG_{U_3O_8(s)} - 0.5{}^oG_{O_2(g)} + .{}^o G_{C_{p\_opt}} + 417234 - 268T$
${}^0L_{U^{+5},U^{+6}:O_2^{-2}:O_2^{-2}} = 299521 - 112.6T$
${}^1L_{U^{+5},U^{+6}:O_2^{-2}:O_2^{-2}} = -58424 - 32.5T$
${}^2L_{U^{+5},U^{+6}:O_2^{-2}:O_2^{-2}} = 198764 + 43.1T$
${}^0L_{U^{+5},U^{+6}:O_2^{-2}:Va} = -523128 + 126.2T$
${}^1L_{U^{+5},U^{+6}:O_2^{-2}:Va} = -156283 + 70.7T$
${}^2L_{U^{+5},U^{+6}:O_2^{-2}:Va} = -312004 - 11.5T$

[a] Thermodynamic values for the compound and gas species contributing to endmember Gibbs energies are listed in Table 2

Table 2. Enthalpy, entropy, and heat capacity constant values of specified compound, gas species, and optimization parameter

Compound	T range (K)	$\Delta H_{298.15\ \mathrm{K}}$ (J/mol)	$S_{298.15\ \mathrm{K}}$ (J/mol·K)	C_p[a] constants				Reference
				a	b	c	d	
U_3O_8(s)	298.15 < T < 6000	-3576818.45	285.022053	276.747750	27.328834	-40.733348		Guéneau et al[4]
O_2(g)	298.15 < T < 1000	0	205.033	22.271	20.3955	1.53460	-7942.149996	Guéneau et al[4]
	1000 < T < 3300			33.6276	2.38319	-10.51620	-81.372	
	3300 < T < 6000			37.9072	1.700972	-175.328	-128.652	
C_p_opt	298.15 < T < 2000	0	0		-133.6			Optimization[b]

[a] $C_p\ (\mathrm{J/mol \cdot K}) = a + b \cdot 10^{-3}T + c \cdot 10^{5}T^{-2} + d \cdot 10^{-9}T^{2}$

[b] Value obtained by optimizing to $UO_{2.667}$ heat capacity data[37] (Section 3.2.1)

Table 3. Oxygen stoichiometry of U_3O_{8-x} at specified temperatures in U-O system (Figs. 2 & 5)

T (K)	O stoichiometry of U_3O_{8-x}
1148	7.9530
1173	7.9468
1198	7.9408

8. References

1. Momeni M. H., Kisieleski W. E., Rayno D. R., et al., Radioisotopic composition of yellow cake. An estimation of stack release rates. ANL/ES-84, Argonne National Laboratory, Argonne, Il, 1979. 1-32.

2. Morel B., Amaraggi D., Arab M., et al., Method for converting UO_3 or U_3O_8 into hydrated UO_4, US 9,045,350 B2. 2015.

3. Guéneau C., Baichi M., Labroche D., et al., Thermodynamic assessment of the uranium–oxygen system. *J. Nucl. Mater.* 2002;304:161-175.

4. Guéneau C., Dupin N., Sundman B., et al., Thermodynamic modelling of advanced oxide and carbide nuclear fuels: Description of the U–Pu–O–C systems. *J. Nucl. Mater.* 2011;419:145-167.

5. ASTM, Standard test method for the determination of uranium by ignition and the oxygen to uranium (o/u) atomic ratio of nuclear grade uranium dioxide powders and pellets, ASTM C1453-00. ASTM International, West Conshohocken, PA, 2011. 1-3.

6. Matsui T., Tsuji T., Naito K., New phase transitions in non-stoichiometric U_3O_{8-x} at high temperatures, (I). *Journal of Nuclear Science and Technology.* 1974;11:216-222.

7. Ackermann R. J., Chang A. T., Thermodynamic characterization of the U_3O_{8-z} phase†. *The Journal of Chemical Thermodynamics.* 1973;5:873-890.

8. Blackburn P. E., Oxygen dissociation pressures over uranium oxides. *J. Phys. Chem.-US.* 1958;62:897-902.

9. Grønvold F., High-temperature x-ray study of uranium oxides in the UO_2-U_3O_8 region. *Journal of Inorganic and Nuclear Chemistry.* 1955;1:357-370.

10. Fujino T., Tagawa H., Adachi T., On some factors affecting the nonstoichiometry in U_3O_8. *J. Nucl. Mater.* 1981;97:93-103.

11. Goto K., Composition of uranium oxides heated in the air. *Nippon Kagaku Zassi.* 1968;89:927-929.

12. Dharwadkar S. R., Chandrasekharaiah M. S., Karkhanavala M. D., A physicochemical study of the uranium-oxygen system between $UO_{2.65}$ and $UO_{2.67}$. *J. Nucl. Mater.* 1978;71:268-276.

13. Kotlar A., Gerdanian P., Dode M., Détermination des pressions partielles d'oxygène en équilibre avec les oxydes non-stoechiométriques du système U-O pour $1050^oC < \theta < 1150^oC$ et $2{,}19 < O/U < 2{,}63$. II. - Tracé des isothermes P_{O2} (O/U) pour 1082^oC - 1098^oC - 1123^oC - 1137^oC et 1150^oC. Diagramme des phases. *J. Chim. Phys.-Chim. Biol.* 1967;64:1135-+.

14. Kozhina I. I., Shiryaeva L. V., Investigation of the uranium-oxygen phase diagram in the composition region from $UO_{2.25}$ to $UO_{2.67}$. *Radiokhimiya.* 1974;16:360-363.

15. Andersson J. O., Guillermet A. F., Hillert M., et al., A compound-energy model of ordering in a phase with sites of different coordination numbers. *Acta Metall. Mater.* 1986;34:437-445.

16. Havrig H., An extended version of the regular solution model for stoichiometric phases and ionic melts. *Acta Chem. Scand.* 1971;25:3199-3204.

17. Hillert M., Staffansson L. I., Regular solution model for stoichiometric phases and ionic melts. *Acta Chem. Scand.* 1970;24:3618-3626.

18. Sundman B., Agren J., A regular solution model for phases with several components and sublattices, suitable for computer applications. *J. Phys. Chem. Solids.* 1981;42:297-301.

19. Hillert M., The compound energy formalism. *J. Alloy Compd.* 2001;320:161-176.

20. Hillert M., Some properties of the compound energy model. *Calphad-Comput. Coupling Ph. Diagrams Thermochem.* 1996;20:333-341.

21. Lukas H., Fries S. G., Sundman B., Computational thermodynamics: The calphad method, 1sted. New York, NY: Cambridge University Press; 2007.

22. Bale C. W., Bélisle E., Chartrand P., et al., FactSage thermochemical software and databases, 2010–2016. *CALPHAD.* 2016;54:35-53.

23. Naito K., Inaba H., Takahashi S., Phase transitions in U_3O_{8-z}: I, heat capacity measurements. *J. Nucl. Mater.* 1982;110:317-323.

24. Naito K., Tsuji T., Ohya F., Phase transitions in U_3O_{8-z}: II. Electrical conductivity measurement. *J. Nucl. Mater.* 1983;114:136-142.

25. Herak R., The crystal structure of the high temperature modification of U_3O_8. *Acta Crystallographica Section B.* 1969;25:2505-2508.

26. Loopstra B. O., The phase transition in α-U_3O_8 at 210°C. *Journal of Applied Crystallography.* 1970;3:94-96.

27. Ackermann R. J., Chang A. T., Sorrell C. A., Thermal expansion and phase transformations of the U_3O_{8-z} phase in air. *Journal of Inorganic and Nuclear Chemistry.* 1977;39:75-85.

28. Desgranges L., Baldinozzi G., Rousseau G., et al., Neutron diffraction study of the in situ oxidation of UO_2. *Inorg. Chem.* 2009;48:7585-7592.

29. Loopstra B. O., Neutron diffraction investigation of U_3O_8. *Acta Crystallographica.* 1964;17:651-654.

30. Zachariasen W. H., Crystal chemical studies of the 5f-series of elements .I. New structure types. *Acta Crystallographica.* 1948;1:265-269.

31. Chodura B., Maly J., A contribution to the solution of the structure of U_3O_8. *J. Inorg. Nucl. Chem.* 1958;7:177-178.

32. Andresen A., The structure of U_3O_8 determined by neutron diffraction. *Acta Crystallographica.* 1958;11:612-614.

33. Ball R. G. J., Dickens P. G., Calculation of structural and defect properties of α-U_3O_8. *J. Mater. Chem.* 1991;1:105-112.

34. Brincat N. A., Parker S. C., Molinari M., et al., Density functional theory investigation of the layered uranium oxides U_3O_8 and U_2O_5. *Dalton Trans.* 2015;44:2613-2622.

35. Kvashnina K. O., Butorin S. M., Martin P., et al., Chemical state of complex uranium oxides. *Phys. Rev. Lett.* 2013;111:5.

36. Teterin Y. A., Teterin A. Y., The structure of the x-ray photoelectron spectra of light actinide compounds. *Uspekhi Khimii.* 2004;73:588-631.

37. Inaba H., Shimizu H., Naito K., Lambda-type heat capacity anomalies in U_3O_8. *J. Nucl. Mater.* 1977;64:66-70.

38. Gronvold F., Crystal structure of uranium oxide (U_3O_8). *Nature.* 1948;162:70-70.

39. George A. M., Karkhanavala M. D., Studies of the electrical properties of uranium oxides - I. Electrical conductivity of α-U_3O_8. *J. Phys. Chem. Solids.* 1963;24:1207-1212.

40. Matsui T., Naito K., Phase relation and defect structures of nonstoichiometric $U_4O_{9\pm y}$ and UO_{2+x} at high-temperatures. *J. Nucl. Mater.* 1975;56:327-335.

41. Caneiro A., Abriata J. P., Equilibrium oxygen partial pressure and phase diagram of the uranium-oxygen system in the composition range 2.61 < O/U < 2.67 between 844 and 1371 K. *J. Nucl. Mater.* 1984;126:255-267.

42. Labroche D., Dugne O., Chatillon C., Thermodynamic properties of the O-U system. II - Critical assessment of the stability and composition range of the oxides UO_{2+x}, U_4O_{9-y} and U_3O_{8-z}. *J. Nucl. Mater.* 2003;312:50-66.

43. Dorogokupets P. I., Equation of state for lambda transition in quartz. *Journal of Geophysical Research: Solid Earth.* 1995;100:8489-8499.

44. Binder K., Theory of first-order phase transitions. *Reports on Progress in Physics.* 1987;50:783-859.

45. Cox A. N., Allen's Astrophysical Quantities, 4ed. New York New York: Springer-Verlag New York; 2002.

46. Tempest P. A., Tucker P. M., Tyler J. W., Oxidation of UO_2 fuel pellets in air at 503 and 543 K studied using X-ray photoelectron spectroscopy and X-ray diffraction. *J. Nucl. Mater.* 1988;151:269-274.

47. Cox D. S., Hunt C. E. L., O'Connor R. F., et al., High-temperature oxidation behaviour of UO_2 in air and steam, 198-211. in High-Temperature Oxidation and Sulphidation Processes**.** Edited by J. D. Embury. Pergamon, Oxford, 1990.

48. Leinders G., Ozdemir O., Pakarinen J., et al., Oxidation of UO_2 in dry and wet atmospheres, Top Fuel. Prague, Czech Republic, 2018. 1-7.

Highlights

- U_3O_{8-x} phase was thermodynamically modeled as a solid solution for the first time
- The U-O binary phase diagram was calculated/plotted with the U_3O_{8-x} phase
- Revised ASTM C 1453 U_3O_8 to U conversion factor computed using U_3O_{8-x} model

Declaration of interests

☒ The authors declare that they have no known competing financial interests or personal relationships that could have appeared to influence the work reported in this paper.

☐The authors declare the following financial interests/personal relationships which may be considered as potential competing interests: